J. At. Mol. Sci.
doi: 10.4208/jams.081109.091809a

Vol. **1**, No. 2, pp. 143-151
May 2010

Elastic and optical properties of CeO_2 via first-principles calculations

Li-Li Sun[a], Yan Cheng[a,*], and Guang-Fu Ji[b,*]

[a] *School of Physical Science and Technology, Sichuan University, Chengdu 610064, China*
[b] *Laboratory for Shock Wave and Detonation Physics Research, Institute of Fluid Physics, Chinese Academy of Engineering Physics, Mianyang 621900, China*

Received 11 August 2009; Accepted (in revised version) 18 September 2009;
Available online 19 April 2010

Abstract. The elastic and optical properties of the cubic CeO_2 and its behavior under pressure are investigated by using the local density approximation (LDA). The computational results are found in good agreement with the available experimental data and other theoretical results. The optical properties including dielectric function, absorption, reflectivity and refractive index are calculated and analyzed. It is found that CeO_2 is transparent from the partially ultra-violet to the visible light area and the transparence is hardly affected by the pressure. Furthermore, the curve of optical spectrum shifts to high energy area (blue shift) with increasing pressure.

PACS: 71.15.Mb, 62.20.dq, 78.20.Ci
Key words: density functional theory, elastic properties, optical properties, CeO_2

1 Introduction

As a rare-earth oxide, cerium oxide forms an interesting and extensively studied series, and has numerous applications in technology. For example, as one of the non-stoichiometric oxides [1], CeO_2 is extensively used in the modern catalytic industry due to its high oxygen storage capability [2–7]. It is the major component in catalytic converters to reduce harmful emissions from automobile exhausts [2], and has been often used as a promoter in an automotive exhaust catalyst for purifying carbon monoxide (CO), nitrogen oxides (NO_x) and hydrocarbon (HC) [4–9]. The automotive catalyst system has been operated under the conditions of a certain range of air/fuel (A/F) ratio . The CeO_2 can provide oxygen for oxidizing CO and HC under rich A/F conditions, and remove it

*Corresponding author. *Email address:* yan.cheng@126.com (Y. Cheng); cyfjkf@caep.ac.cn (G. F. Ji)

from the exhaust gas phase for reducing NO_x under lean A/F conditions [10]. It is also found that the CeO_2 is of the potential interest as optical component materials and laser hosts [11–14] and as prospective materials for future microelectronic applications [15].

Although CeO_2 has long been utilized as a material for oxygen storage [2–7], first-principles calculations on CeO_2 have hitherto been prohibitive, not least because of the difficulty in describing or converging the localized f valence electrons [16]. As fundamental issues and key features of cerium oxides CO_2, like the occupation of the $4f$ orbital and bonding, have been investigated by a number of experimental techniques [11,17]. In the early 1980s, Koelling *et al.* [18] calculated the electronic structure of CeO_2 by means of the linear augmented-plane wave (LAPW) method with Slater exchange and warped muffin-tin approximation for the crystal potential and charge density. They reported that the f and d states of Ce atom are hybridized with the oxygen $2p$ bands.

Hill and Catlow [19] investigated CeO_2 by the restricted Hartree-Fock method, which is well known for describing the exchange interaction correctly but entirely missing the correlation effects [20]. More recently, Skorodumova *et al.* [21] have calculated the electronic, structural, bonding, optical and magnetic properties of CeO_2 by means of the full-potential linear muffin-tin orbital (FP-LMTO) method in the framework of the density functional theory (DFT). They showed that in the case of CeO_2 their calculated density of states, optical transitions and electron localization function indicate that the unoccupied $4f$ states of Ce can be considered as essentially equivalent to an empty atomic like $4f$ level. Also, Fabris *et al.* [22] investigated on the defective CeO_2 by modeling multiple valence compounds using density-functional theory.

In this work, we give a detailed description for the elastic and the optical properties of CeO_2 through the Cambridge Serial Total Energy Package (CASTEP) program [23,24]. The structure and elastic constants obtained here are in agreement with the experimental data and other theoretical results. The elastic and optical properties of CeO_2 as well as their behavior under pressure have also studied.

2 Theoretical method

2.1 Total energy electronic structure calculations

In our electronic structure calculations, we adopt the non-local ultrasoft pseudopotential introduced by Vanderbilt [25] for the interactions of the electrons with the ion cores, together with the local density approximation (LDA) [26]. The electronic wave functions are expanded in a plane wave basis set with energy cut-off of 480 eV. For the Brillouin-zone k-point sampling, we use the Monkhorst-Pack mesh with $10\times10\times10$ k-points. It is found that these parameters are sufficient in leading to well converged total energy, geometrical configurations and elastic stiffness coefficients.

2.2 Elastic properties

The elastic stiffness tensor relates to the stress tensor and the strain tensor by Hooke's law. Since the stress and strain tensors are symmetric, the most general elastic stiffness tensor has only 21 non-zero independent components. For a cubic crystal, they are reduced to three components, *i.e.*, C_{11}, C_{12}, and C_{44}. These elastic constants can be determined by computing the stress generated by forcing a small strain to an optimized unit cell [27,28]. Moreover, the adiabatic bulk B_S and the shear modulus G are given by

$$B_S=\frac{1}{3}(C_{11}+2C_{12}),\quad G=\frac{1}{2}(G_V+G_R),$$

where

$$C=\frac{1}{2}(C_{11}-C_{12}),\quad G_V=\frac{1}{5}(2C+3C_{44}),\quad G_R=\frac{15}{6/C+9/C_{44}},$$

G_V is the Voigt shear modulus and G_R is the Reuss shear modulus [29]. For cubic crystals, the mechanical stability of crystals under pressure P is judged by

$$\widetilde{C}_{44}>0,\quad \widetilde{C}_{11}>|\widetilde{C}_{12}|,\quad \widetilde{C}_{11}+2\widetilde{C}_{12}>0,$$

where $\widetilde{C}_{\alpha\alpha}=C_{\alpha\alpha}-P$ ($\alpha=1,4$), $\widetilde{C}_{12}=C_{12}+P$ [30]. Moreover, the internal strain parameter ξ can be obtained from the relation [31]

$$\xi=\frac{C_{11}+8C_{12}}{7C_{11}+2C_{12}}.$$

As an important physical quantity, the Debye temperature is closely related to the elastic constants. From the elastic constants, one can obtain the elastic Debye temperature. The Debye temperature may be estimated from the following formulas [32]

$$\Theta=\frac{\hbar}{k}\left[\frac{3n}{4\pi}\left(\frac{N_A\rho}{m}\right)\right]^{1/3}V_m, \tag{1}$$

where V_m is the average sound velocity, $\hbar$ the Planck'sconstant, k the Boltzmann's constant, N_A the Avogadro's number, n the number of atoms per formula unit, M the molecular mass per formula unit, $\rho(=M/V)$ is the density, and V_m is obtained from

$$V=\left[\frac{1}{3}\left(\frac{2}{V_S^3}+\frac{1}{V_L^3}\right)\right]^{-1/3}, \tag{2}$$

where V_S and V_L are the shear and longitudinal sound velocities, respectively. The probable values of the average shear and longitudinal sound velocities can be calculated from the Navier's equation [33]

$$V_S=\sqrt{\frac{G_H}{\rho}}, \tag{3}$$

$$V_L=\sqrt{\frac{\left(B_H+\frac{4}{3}G_H\right)}{\rho}}. \tag{4}$$

2.3 Optical properties

Generally, the optical properties of a material can be described by many physical parameters, including complex refractive index N, absorption coefficient π, reflectivity coefficient R, optical conductivity σ, complex dielectric constant ε, and so on. All the optical constants can be derived from the real part $\varepsilon_1(\omega)$ and image part $\varepsilon_2(\omega)$ of the the complex frequency-dependent dielectric function $\varepsilon(\omega)=\varepsilon_1(\omega)+i\varepsilon_2(\omega)$. The imaginary or absorptive part $\varepsilon_2(\omega)$ of the frequency-dependent dielectric function is given by [34]

$$\varepsilon_2(\omega)=\frac{e^2\hbar}{\pi m^2\omega^2}\sum_{v,c}\int_{BZ}|M_{cv}(\kappa)|^2\delta[\omega_{cv}(k)-\omega]d^3k. \tag{5}$$

The integral is carried out over the first Brillouin zone, and the momentum dipole elements $M_{vk}(k)=<u_{cv}|e\cdot\nabla|u_{ck}>$, where e is the potential vector defining the electric field, are matrix elements for direct transitions between valence-band $u_{vk}(r)$ and conduction-band $u_{ck}(r)$ states, and the

$$\hbar\omega_{cv}(k)=E_{ck}-E_{vk}$$

is the corresponding transition energy.

The real part $\varepsilon_1(\omega)$ of the frequency-dependent dielectric function can be derived from the imaginary part using the Kramers-Kronig relations

$$\varepsilon_1(\omega)=1+\frac{2}{\pi}p\int_0^\infty\frac{\omega'\varepsilon_2(\omega')}{\omega'^2-\omega^2}d\omega', \tag{6}$$

where P denotes the principal value of the integral. Based on the knowledge of both real and imaginary parts of the frequency-dependent dielectric function, we can calculate the important optical functions such as the refractive index $n(\omega)$

$$n(\omega)=\left(\frac{\varepsilon_1(\omega)}{2}+\frac{\sqrt{\varepsilon_1^2(\omega)+\varepsilon_2^2(\omega)}}{2}\right)^{1/2}. \tag{7}$$

In order to investigate the optical properties, a sufficiently dense k-mesh is used in the present work.

3 Results and discussion

3.1 Structure and elastic properties

Cerium oxide CeO_2 has the fluorite structure with three atoms per primitive face-centered-cubic cell; Ce is located at $(0,0,0)$ while two oxygen atoms are at $\pm(1/4,1/4,1/4)$ reduced positions. First of all, we calculate the equilibrium properties of CeO_2 for the sake of judging whether the computational methodology is reliable and effective. Together with

Table 1: Calculated equilibrium lattice parameter a (Å), bulk modulus B_0 (GPa)and its pressure derivative B_0', and elastic constants C_{ji}(GPa) of CeO_2 together with the experimental data and other theoretical results.

	a	B_0	B_0'	C_{11}	C_{12}	C_{44}	ξ	B_s
Present	5.37	203.59	4.41	371.40	117.89	68.10	0.46	202.40
Expt. [35]		204		403	105	60		
Expt. [36]	5.411	220	4.4					
Ref. [37]	5.39	214.7						
Ref. [38]	5.45	193.5						
Ref. [39]	5.366	210.1	4.4	386	124	73		

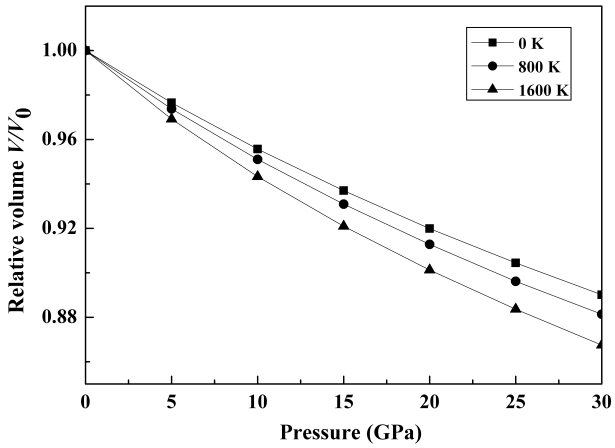

Figure 1: Relative volume versus pressure of CeO_2 at 0 K, 800 K and 1600 K, respectively.

the experimental data and other theoretical results, the calculated ground state properties, i.e., the equilibrium lattice constant, bulk module B_0 and its pressure derivative B_0', and elastic constants of CeO_2 are given in Table 1. The obtained results and its pressure derivative B_0' are in excellent agreement with the experimental values and other theoretical results.

The pressure and temperature dependences of the relative volume V/V_0 of CeO_2 are illustrated in Fig. 1. It is seen that, as the pressure P increases, the relative volume V/V_0 decreases at a given temperature, and the relative volume V/V_0 of higher temperature is less than that of lower temperature at the same pressure. On the other hand, the volume V decreases with the elevated pressure P, and increases with the elevated temperature T. This effect of increasing pressure on CeO_2 is just the same as decreasing temperature.

In Table 2, we present the pressure dependences of the elastic constants C_{ij}, the aggregate elastic modulus B, G of CeO_2 at 0-30 GPa. Unfortunately, no experimental and

Table 2: Calculated lattice parameters a (Å), elastic constants C_{ij}(GPa) and aggregate elastic moduli B(GPa), B_0', shear modulus G(GPa), Debye temperature Θ (K), and anisotropic factor Δ_{S1} of CeO_2 under pressure P (GPa).

P	a	C_{11}	C_{12}	C_{44}	B	B_0'	G	Θ	Δ_{S1}
0	5.37	371.40	117.89	68.10	203.59	4.41	87.65	503.76	1.86
5	5.34	395.77	136.85	73.55	223.16	4.29	92.41	516.45	1.76
10	5.30	421.54	158.03	79.43	245.87	4.18	97.39	528.78	1.66
15	5.27	445.45	177.75	85.67	266.98	4.09	102.51	541.03	1.56
20	5.23	467.91	196.40	91.45	286.88	4.01	109.06	551.83	1.48
25	5.20	490.51	215.37	96.97	307.08	3.94	111.58	561.73	1.42
30	5.18	511.28	233.13	101.35	325.85	3.87	115.06	569.25	1.37

theoretical data of elastic constants are available for our comparison. It is shown from Table 2 that the elastic constants C_{11}, C_{12}, C_{44}, bulk modulus B and shear modulus G increase monotonously when pressure is enhanced. Moreover, C_{44} and G increase very slowly with the elevated pressure. It is noted that the Debye temperature of CeO_2 tend to increase with increasing pressure. On the other hand, for the shear waves of CeO_2, the wave polarized perpendicular to the basal plane ($S1$) and the one polarized in the basal plane ($S2$) have the anisotropies

$$\Delta_{S1} = \frac{1}{\Delta_{S2}} = \frac{C_{11} - C_{12}}{2C_{44}}. \tag{8}$$

In Table 2, we also list the calculated Δ_{S1}. It is noted that, Δ_{S1} generally descends as pressure increases from 0 to 30 GPa. As pressure increases, the anisotropy will weaken.

3.2 Optical properties

In Fig. 2(a), we display the imaginary part of dielectric function curves to the photon energy from 0 to 40 eV at 0 and 30 GPa. It can be found that, at 0 GPa, there are two pronounced peaks E_1 and E_2 localized at 2.85 eV and 10.11 eV, respectively, and one weak peak E_3 at 22.33 eV in $\varepsilon_2(\omega)$. The three peaks all decrease and shift to the right with a small extent when the applied pressure is up to 30 GPa. When compared with Figs. 2(b) and 2(c), we found that in the area where absorption is intense the reflectivity is also larger. That means if a kind of material can absorb light in some range strongly it can effectively reflect the same area light too. At 0 GPa, it is noted that there is a lossless region from 0 to about 1.46 eV in absorption spectrum, and in the lossless region the reflectivity is lower than 20%, indicating that just the frequency less than 1.46 eV can be transmitted in CeO_2.

Further more, the reflectivity for frequency at about 13 eV is even high than 60%, but a sharp decrease happens subsequently. Then, at about 27.8 eV there is a peak too, but is only 28%. When the pressure increased to 30 GPa, the absorption became more intense

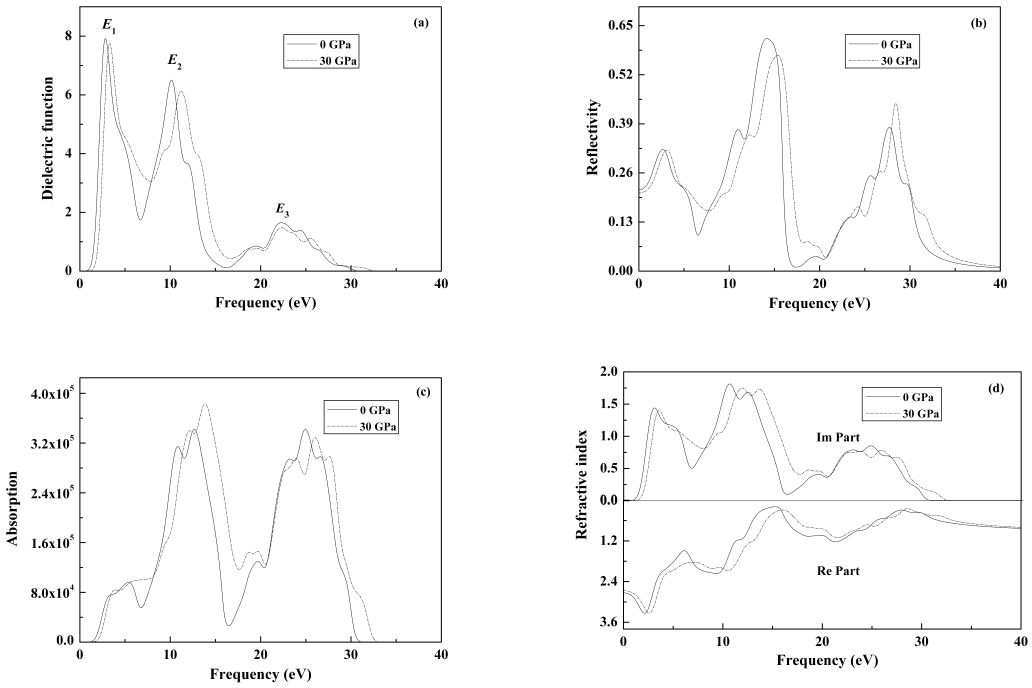

Figure 2: Optical properties of CeO_2 at 0 GPa (solid line) and 30 GPa (dashed): (a) Dielectric function, (b) Reflectivity, (c) Absorption spectra, and (d) Refractive index.

and the reflectivity decreased accordingly. For the study of pressure induced influence on optical properties of CeO_2, complex refractive index is also an important objective. In Fig. 2(d), both the real and imaginary part of complex refractive index at 0 and 30 GPa are illustrated. Obviously, at high-energy region, where photon energy is larger than about 28 eV, the values of imaginary part are very small even close to zero. The result suggests that for the high frequency electromagnetic wave the absorption is very weak, and the refractive index is almost constant at high frequency area, indicating that the CeO_2 is transparent from the ultra-violet (mainly UV-A, UV-B and partially UV-C) to the visible light area and it seems that hardly does the transparence affected by the pressure. Compared with Fig. 2(a) to Fig. 2(d), it is found that the pressure has little effect on the shape of optical spectrum curve, but the positions of the peaks are moved towards the higher energy direction.

4 Summary

In summary, we give a detailed description for the elastic and the optical properties of CeO_2 and their behavior under pressure by using *ab initio* plane-wave pseudopotential

density functional theory method within the local density approximation (LDA). The calculated results are in good agreement with the available experimental data and other theoretical results reasonably. The optical properties including dielectric function, absorption, reflectivity and refractive index are also calculated and analyzed. It is found that the CeO_2 is transparent from the partially ultra-violet to the visible light area and hardly does the transparence affected by the pressure. Furthermore, the curve of optical spectrum will shift to high energy area (blue shift) with increasing pressure.

Acknowledgments. The authors thank the supports by the National Natural Science Foundation of China under Grant No. 10776022, and by the Specialized Research Fund for the Doctoral Program of Higher Education under Grant No. 20090181110080. We also thank the support by the Youth Science Foundation of Sichuan University under Grant No. 2008131. All calculations are performed using the computational resources by the State Key Laboratory of Polymer Materials Engineering of China in Sichuan University.

References

[1] D. J. M. Beven and J. Kordis, J. lnorg. Nucl. Chem. 26 (1964) 1509.
[2] M. S. Dresselhaus and I. L. Thomas, Nature 414 (2001) 332.
[3] T. Hibino, A. Hashimoto, T. Inoue, J. Tokuno, S. Yoshida, and M. Sano, Science 288 (2000) 2031.
[4] Y. F. Yu-Yao and J. T. Kummer, J. Catal. 106 (1987) 307.
[5] H. C. Yao and Y. F. Yu-Yao, J. Catal. 86 (1984) 254.
[6] E. C. Su, C. N. Montreuil, and W. G. Rothschild, Appl. Catal. 17 (1985) 75.
[7] R. K. Herz and J. A. Sell, J. Catal. 94 (1985) 166.
[8] J. C. Schlatter and P. J. Mitchell, Ind. Eng. Chem. Prod. Res. Dev. 19 (1980) 288.
[9] G. Kim, Ind. Eng. Chem. Prod. Res. Dev. 21 (1982) 267.
[10] M. Ozawa, M. Kimura, and A. Isogal, J. Mater. Science 26 (1991) 4818.
[11] F. Marabelli and P. Wachter, Phys. Rev. B 36 (1987) 1238.
[12] S. Guo, H. Arwin, S. N. Jacobsen, K. Jarrendahl, and U. Helmersson, J. Appl. Phys. 77 (1995) 5369.
[13] M. Niwano, S. Sato, T. Koide, T. Shidara, A. Fujimori, H. Fukutani, S. Shin, and M. Ishigame, J. Phys. Soc. 57 (1988) 1489.
[14] M. Veszelei, L. Kullman, C. G. Granqvist, N. Rottkay, and M. Rubin, Appl. Optim. 37 (1998) 5993.
[15] T. Yamamoto, H. Momida, T. Hamada, T. Uda, and T. Ohno, Thin Solid Film 486 (2005) 136.
[16] C. J. Pickard and M. C. Payne, Phys. Rev. Lett. 85 (2000) 5122.
[17] A. Fujimori, Phys. Rev. B 27 (1983) 3992.
[18] D. D. Koelling, A. M. Boring, and J. H. Wood, Solid State Commun. 47 (1983) 227.
[19] S. E. Hill and C. R. A. Catlow, J. Phys. Chem. Solids 54 (1993) 411.
[20] S. Mehrotra, P. Sharma, M. Rajagopalan, and A. K. Bandyopadhyay, Solid State Commun. 140 (2006) 313.
[21] N. V. Skorodumova, R. Ahuja, S. I. Simak, I. A. Abrikosov, B. Johansson, and B. I. Lundqvist, Phys. Rev. B 64 (2001) 115108.
[22] S. Fabris, S. de Gironcoli, S. Baroni, G. Vicario, and G. Balducci, Phys. Rev. B 71 (2005) 041102.

[23] M. C. Payne, M. P. Teter, D. C. Allen, T. A. Arias, and J. D. Joannopoulos, Rev. Mod. Phys. 64 (1992) 1045.
[24] V. Milan, B. Winker, J. A. White, C. J. Packard, M. C. Payne, E. V. Akhmatskaya, and R. H. Nobes, Int. J. Quant. Chem. 77 (2002) 85.
[25] D. Vanderbilt, Phys. Rev. B 41 (1990) 7892.
[26] J. P. Perdew and Y. Wang, Phys. Rev. B 45 (1992) 13244.
[27] B. B. Karki, L. Stixrude, S. J. Clark, M. C. Warren, G. J. Ackl, and J. Crain, Am. Miner. 82 (1997) 51.
[28] R. M. Wentzcovitch, N. L. Ross, and G. D. Price, Phys. Earth Planet. Inter. 90 (1995) 101.
[29] C. S. Zha, H. K. Mao and R. J. Hemley, Proc. Natl. Acad. Sci. USA 97 (2000) 13494.
[30] G. V. Sinko and N. A. Smirnow, J. Phys.: Condens. Matter 14 (2002) 6989.
[31] M. B. Kanoun, A. E. Merad, J. Cibert, H. Aourag, and G. Merad, J. Alloys Compnd. 366 (2004) 86; A. E. Merad, H. Aourag, B. Khalifa, C. Mathieu, and G. Merad, Superlatt. Microstruct. 30 (2001) 241.
[32] O. L. Anderson, J. Phys. Chem. Solids 24 (1963) 909.
[33] E. Schreiber, O. L. Anderson, and N. Soga, Elastic Constants and Their Measurements (McGraw-Hill, New York, 1973).
[34] C. Amrosch-Draxl and J. O. Sofo, Comput. Phys. Commun. 175 (2006) 1.
[35] A. Nakajima, A. Yoshihara, and M. Ishigame, Phys. Rev. B 50 (1994) 13297.
[36] L. Gerward, J. S. Olsen, L. Petit, G. Vaitheeswaran, V. Kanchana, and A. Svane, J. Alloys Compnd. 400 (2005) 56.
[37] N. V. Skorodumova, R. Ahuja, S. I. Simak, I. A. Abrikosov, B. Johansson, and B. I. Lundqvist, Phys. Rev. B 64 (2001) 115108.
[38] Z. Yang, T. K. Woo, M. Baudin, and K. Hermansson, J. Chem. Phys. 120 (2004) 7741.
[39] T. Gürel and R. Eryiğit, Phys. Rev. B 74 (2006) 014302.